IEICE TRANS. COMMUN., VOL.E94–B, NO.8 AUGUST 2011

PAPER

Imaging Radio-Frequency Power Distributions by an EBG Absorber

Satoshi YAGITANI[†a)], ***Member***, **Keigo KATSUDA**[†], ***Student Member***, **Masayuki NOJIMA**[†], ***Nonmember***, **Yoshiyuki YOSHIMURA**[††], ***Member***, ***and*** **Hirokazu SUGIURA**[††], ***Nonmember***

SUMMARY A thin electromagnetic band-gap (EBG) absorber is employed to capture the 2-d image of radio-frequency (RF) power distribution. The EBG absorber consists of an array of mushroom unit cells formed on a thin dielectric substrate with a metal backplane, and lumped resistors interconnecting the surface patches of the mushrooms. Around the resonance frequency at which the EBG structure acts as a high-impedance surface, the RF power incident on the surface is absorbed by the lumped resistors which are matched with the incident wave impedance. By detecting directly the amounts of power consumed by the individual resistors, an "RF power imager" can be constructed which captures the 2-d distribution of the RF power illuminating the EBG surface, where polarization discrimination is possible. The resonance (i.e., absorption) frequency is made tunable by adding varactor diodes in parallel with the lumped resistors. The EBG absorber tunable in the frequency range of 700 MHz–2.7 GHz is designed and fabricated, and its performance is evaluated by an equivalent-circuit analysis, simulation and measurement. It is shown that the small resistance of the varactors have a considerable effect on the absorption performance. RF power distributions radiated from a dipole antenna are successfully measured by a matrix of sensitive power detectors installed on the backside of the absorber. Using such an RF power imager, the power distributions of even impulsive RF signals and/or noises can be captured and visualized in situ and in real-time, while the electromagnetic environment is almost undisturbed by the EBG absorber.

key words: *EBG, absorber, RF power distribution, measurement, imaging*

1. Introduction

In-situ monitoring of the spatial distributions of a radio-frequency (RF) field gives us information useful for localizing and identifying RF noise sources in electronic equipment under actual operating conditions, as well as for evaluating the performance of antennas mounted on wireless communication devices used in real environments. Conventionally, the spatial distributions of the RF field have been measured by antenna positioners, which mechanically scan a volume of interest with a single sensor or a sensor array. As the scanning takes a certain time to complete, it is generally difficult to obtain "snapshots" of the 2-d or 3-d spatial field distributions, particularly for impulsive signals and/or noises showing up for a brief instant much shorter than the scanning time. A further concern is that the sensor itself may disturb the actual electromagnetic environment during measurement.

Recently, a couple of new "RF field imaging" techniques were proposed. A "live electro-optic imaging" system was developed to take a video image of electric near-field distributions at microwave frequencies [1]. This system used a sensing light beam modulated by an electro-optic (EO) crystal plate with the electric near-fields applied. The spatial pattern of EO modulation were detected by a 2-d photo-detector array, which down-converted the frequency of modulation with a ultra-parallel photonic heterodyne. While keeping the electromagnetic environment undisturbed, the patterns of electric near-fields of up to a few tens of GHz were lively displayed at a rate as high as 30 frames/second, as a 2-d image with 100×100 pixels. However, the imageable area of the system was limited to just a few centimeters square, and the sensitivity was not high; the minimum detectable RF power input to a microstrip line placed in the vicinity (0.3 mm) of the EO plate was about -1 dBm. On the other hand, an infrared thermography technique was used to obtain the image of the RF power distribution illuminating a wave-absorbing screen [2], where the heat distribution generated by the absorbed RF power was detected. However, high RF power was required to obtain the detectable increase in temperature; even by enhancing the temperature distribution with a lock-in amplifier, it took a couple of minutes to obtain an RF power distribution image over a several centimeters square area illuminated by a microwave transmitter of several hundreds of mW [3].

In the present study we propose a novel technique to capture a live image of RF power distributions incident on an "EBG absorber," which is a thin electromagnetic absorber based on an electromagnetic band-gap (EBG) structure. So far a variety of thin electromagnetic absorbers were designed based on the artificial high-impedance surfaces such as frequency-selective surfaces (FSS) and metamaterial surfaces [4]–[26]. Here the so-called mushroom-type EBG structure is used as the high-impedance surface, which has an array of metallic patches connected to the ground plane by thin vias [27]. When the patches on the surface are interconnected by "lumped resistors" (matched with the free space impedance of 377 Ω), the incident RF power is absorbed by them at the resonance frequency where the EBG structure exhibits a high-impedance feature [9], [10], [13], [21]. We propose to directly measure the power consumed by each of the lumped resistors, which is equivalent to the amount of incident RF power absorbed by that resistor. As

Manuscript received February 1, 2011.
Manuscript revised March 31, 2011.

[†]The authors are with the Graduate School of Natural Science and Technology, Kanazawa University, Kanazawa-shi, 920-1192 Japan.
[††]The authors are with Industrial Research Institute of Ishikawa, Kanazawa-shi, 920-8203 Japan.
a) E-mail: yagitani@is.t.kanazawa-u.ac.jp

DOI: 10.1587/transcom.E94.B.2306

the resistors are arranged in a 2-d matrix, the 2-d distribution of the RF power incident and absorbed on the mushroom surface can be obtained. Since the EBG absorber has inherently a narrow-band absorption feature at the resonance frequency determined by the EBG structure, such an "RF power imager" has a narrow-band frequency response. To extend the measurable frequency range, the resonance frequency is made electronically tunable by additional varactor diodes as in [12], [16], [23], [28]. In the present study a 347-mm square EBG absorber has been designed and fabricated to cover the absorbing frequency range from 700 MHz up to 2.7 GHz. Power distributions are detected at 8×8 locations on the absorber, at each of which two RF power detectors are placed to measure two orthogonal polarizations. By using the sensitive RF power detectors, the minimum detectable power of −70 dBm is achieved. The measured power distributions are transferred to a PC and reconstructed as real-time 2-d power images at a rate of 30 images/second. The frequency range (700 MHz–2.7 GHz) covered by the developed imager includes the multiple frequency bands for mobile phones (800 MHz–2 GHz) and ISM applications (2.4–2.5 GHz) such as wireless LAN systems. By using the imager we can expect to visualize the RF power distributions transmitted from these portable wireless devices used in real environments. The imager could also be applied to identifying RF noise sources on printed circuit boards operating at such high frequencies.

The rest of the paper is organized as follows. In Sect. 2 we describe the basic principle of RF power measurement by an EBG absorber. Section 3 gives the design and performance of the EBG absorber fabricated in the present study, on the basis of an equivalent circuit analysis, simulation, and measurement. Then in Sect. 4 we evaluate the measurement results of RF power distributions radiated by a standard dipole antenna. Section 5 gives a conclusion.

2. Principle of RF Power Measurement by an EBG Absorber

2.1 A Thin Absorber Based on an EBG Structure

Here we construct a thin electromagnetic absorber, by placing lumped resistors on the surface of a mushroom-type EBG structure, as shown in Fig. 1 [9], [10], [13], [21]. The mushroom structure is typically characterized by a periodic array of metal patches, connected to the ground plane by vertical conducting vias through a dielectric thin layer [27]. Lumped resistors are inserted between adjacent patches. The size of each patch, the gap between the patches, and the period of the structure are expressed as w, g and a, respectively. The cross-sectional view of the mushroom structure and its simplified equivalent circuit are shown in Fig. 2. When the size of a unit cell is electrically small (i.e., $a \ll \lambda$), the structure is nearly isotropic and can be treated by an effective medium model [27]. For an electromagnetic wave at normal incidence, the surface impedance of the mushroom structure is then represented as a parallel connection

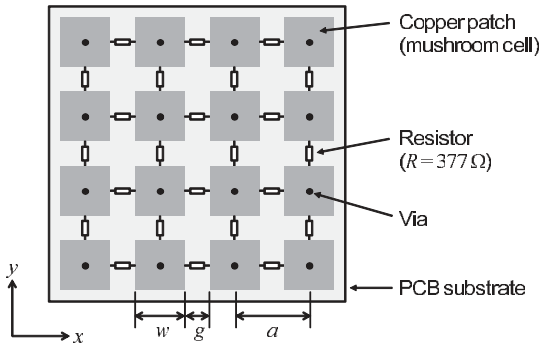

Fig. 1 Geometrical structure of an EBG absorber.

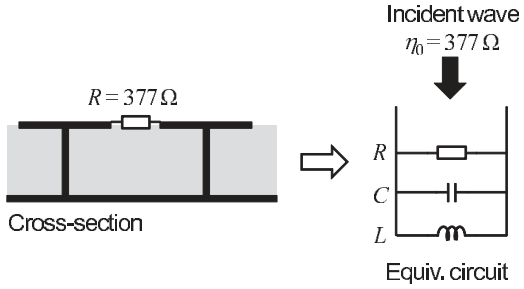

Fig. 2 Simplified model of an EBG absorber.

of the grid impedance of the patch array and the surface impedance of the grounded dielectric slab (cf. [22]), which is more simply approximated as a parallel circuit of the effective inductance L and the effective capacitance C [27]. The high-impedance property is realized at the resonance frequency, where the mushroom layer behaves like an artificial magnetic conductor.

When we insert the lumped resistors R between the adjacent patches, the whole structure is considered as an LCR parallel circuit. For an electromagnetic wave at normal incidence, the reflection coefficient is calculated as

$$\Gamma = \frac{Z_s - \eta_0}{Z_s + \eta_0}, \tag{1}$$

where $\eta_0 = 377\,\Omega$ is the incident wave impedance. At the resonance frequency $\omega_r = 1/\sqrt{LC}$, the surface impedance Z_s becomes purely resistive R. If we take the value of the lumped resistors $R = 377\,\Omega$, then $\Gamma = 0$ and the incident electromagnetic wave should be completely absorbed. The typical frequency variation of the power reflection coefficient, $|\Gamma|^2$, of the EBG absorber is schematically drawn by the solid line in Fig. 3, for the case of the resonance frequency of 1 GHz. The bandwidth of low reflection (high absorption) becomes inherently narrow around the resonance frequency (cf. [22]). The broken line in Fig. 3 plots the power absorption coefficient, $|A|^2 = 1 - |\Gamma|^2$, which exhibits a band-pass-filter feature.

2.2 Detection of Absorbed Power Distribution

On the thin EBG absorber depicted in Fig. 1, the incident

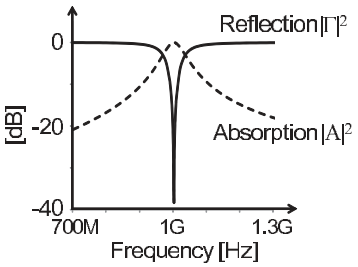

Fig. 3 Typical reflection and absorption characteristics of an EBG absorber.

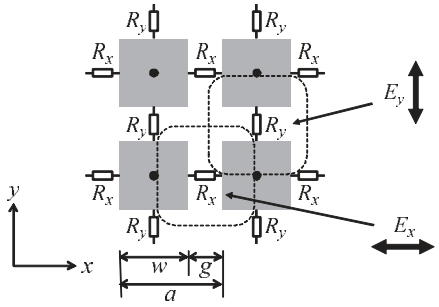

Fig. 4 RF power absorbed by lumped resistors.

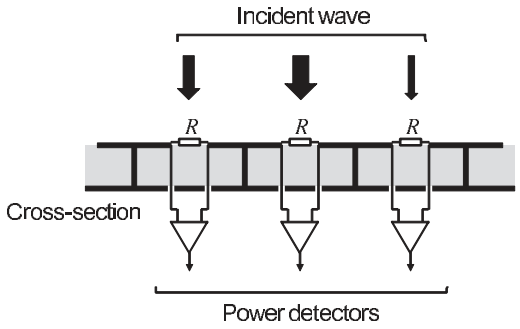

Fig. 5 Detection of RF power absorbed by lumped resistors.

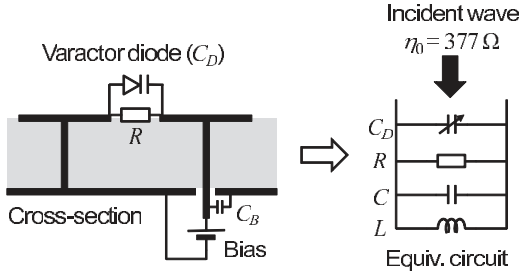

Fig. 6 EBG absorber model with tunable varactor diodes.

wave power is absorbed and dissipated in the surface resistors, when there is no loss in the substrate. For a 2-d matrix of resistors interconnecting the square patches on the surface, the amount of power absorbed by each resistor depends on incident polarizations. Figure 4 shows a part of the EBG surface, where the resistors connecting the adjacent patches in the x- and y-directions are represented as R_x and R_y, respectively. When an RF wave with its electric field (E-field) linearly polarized in the x-axis is normally incident on the surface, its power is absorbed by the resistors R_x. Similarly, a y-polarization is absorbed by R_y. In either case, when the gap g between the patches is much smaller than the cell periodicity a, the power absorbed by each resistor is considered to be $P = S a^2 |A|^2$, where S is the Poynting flux of the incident wave, and a^2 is the area of a unit cell (equivalently the receiving cross section) as indicated by the dotted squares in Fig. 4. When the E-field polarization at normal incidence makes an angle ϕ from the x-axis, its power is divided into P_x and P_y, which are absorbed by R_x and R_y, respectively, as

$$P_x = S a^2 |A|^2 \cos^2 \phi, \quad P_y = S a^2 |A|^2 \sin^2 \phi \,. \tag{2}$$

Thus, each of the resistors on the surface absorbs the amount of power incident on the local area around it. If we measure the power consumption on the individual resistors, we are able to measure the 2-d power distribution of the RF wave illuminating the EBG surface, as well as to identify its polarization. As shown in Fig. 5, power detectors are put on the backside of the EBG absorber, to detect the amounts of power consumed by the individual surface resistors. In this case the power detectors should not alter the surface impedance of the EBG absorber. How to implement such a power detecting circuit will be described later in Sect. 4.1.

2.3 Controlling the Absorption Frequency

As explained in Sect. 2.1, the resonance (absorption) frequency of the EBG absorber is determined by the geometrical and constitutional parameters of the EBG absorber [22], [27]. One of the techniques to make the resonance frequency tunable is to use varactor diodes (varactors). Here we insert a varactor in parallel with each of the surface resistors, thereby altering the capacitance component of the mushroom structure, in the same manner designed by [28]: The varactors are oriented in opposite directions in each alternate row as well as in each alternate column of the matrix of mushrooms. Reverse biases V_R are supplied to all the varactors by alternately biasing half of the cells, and grounding the other half in a checkerboard pattern (see Fig. 3 of [28]). A separate biasing circuit is placed on the backside of the ground plane, as illustrated in the left of Fig. 6, where the capacitor C_B grounds the foot of the biasing via at RF frequencies. As shown by the equivalent circuit in the same figure, the capacitance of the varactor C_D in parallel with the LCR circuit alters the resonance frequency to be

$$\omega_{r,\text{tuned}} = 1/\sqrt{L(C + C_D)} \,. \tag{3}$$

Thus, by applying appropriate bias voltages to the varactors, we can control the frequency of RF power absorption and detection.

3. Design and Performance of an EBG Absorber

3.1 Design

An EBG absorber was designed and fabricated, which has 33 × 33 square unit cells formed on an FR-4 substrate of 347 mm square and 1.6 mm thick. The structure of each unit cell is shown in Fig. 7. The size of a patch is w = 10 mm and the gap between the adjacent patches is g = 0.5 mm, so that the cell periodicity is a = 10.5 mm. The via diameter is 0.6 mm. The patches, the vias and the ground plane are made of copper. The relative permittivity of the FR-4 substrate used here was measured as $\varepsilon_r = \varepsilon_r' - j\varepsilon_r'' = 4.56 - j0.105$ ($\tan\delta = 0.023$).

Lumped resistors and varactor diodes were soldered in parallel between the adjacent patches as in Fig. 7. To achieve good absorption, the surface resistance R_s of the absorber should become as close as possible to $\eta_0 = 377\,\Omega$ at the resonance frequency. It is noted that for the present EBG absorber the value of the lumped resistors R was chosen as 620 Ω, not simply 377 Ω. This is because, as will be explained in detail in Sect. 3.2, R_s depends not only on the dielectric loss [21], but also more significantly on the small series resistance of the varactor [16]. The varactor used here was the silicon tuning diode (Infineon, BB833) [30], which had the actual capacitance range from 0.67 pF (when V_R = 25 V) to 12 pF (0 V). To avoid an unnecessary DC current flowing on the lumped resistors R due to the reverse bias voltage V_R applied on the varactors, we inserted a DC-cut lumped capacitor of 1000 pF in series with each resistor.

3.2 Equivalent Circuit Analysis

Though the basic equivalent circuit of an EBG absorber has been presented in Fig. 6, here we construct a more realistic equivalent circuit of the EBG absorber as in Fig. 8(a), which can accurately explain its absorption performance obtained in the simulation in Sect. 3.4. The varactor is modeled as a series LCR circuit, where C_D is the variable capacitance, L_D is the parasitic inductance, and R_D is the series resistance [16]. According to the datasheet of the varactor BB833 (SOD323 package), typically L_D = 1.8 nH [30]. Due to the existence of the package capacitance, the resistance R_D is dependent on the variable capacitance C_D (i.e., on the reverse voltage V_R). We estimated the value of R_D from the SPICE model and the S_{11} measurement for BB833 which were available from the manufacture site [30]; R_D decreases from 2.2 Ω to about 1.0 Ω when V_R increases from 0 V to 25 V. The inclusion of such L_D and R_D significantly alters the resonance frequency as well as the absorption performance of the EBG absorber [16]. Additionally, L_V = 0.371 nH and L_R = 0.41 nH correspond to the lead inductances of the varactor and the resistor, respectively, when attached on the EBG unit cell. Another inductance L_M = 0.235 nH comes from the current on the patch surface between the varactor and the resistor. The impedance of the

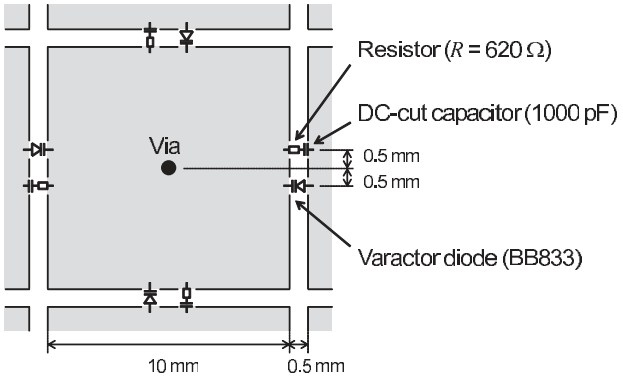

Fig. 7 The unit cell structure on the fabricated EBG absorber.

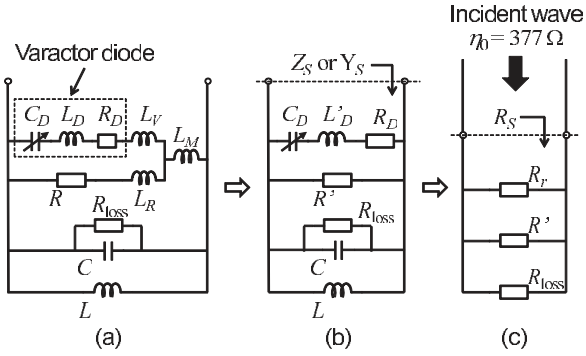

Fig. 8 Equivalent circuit models.

DC-cut capacitance in series with the resistor (see Fig. 7) is so small at high frequencies that it is neglected here.

The effective inductance and capacitance of the mushroom layer were also estimated from the simulation results in Sect. 3.4, as L =1.86 nH and C =0.628 pF, respectively. These values are consistent with, but not exactly the same as, the theoretical values [22], [29]. The dielectric loss of the substrate was represented as the loss resistance calculated by $R_{\rm loss} = 1/\omega C \tan\delta$, which gives $R_{\rm loss}$ = 11 kΩ and 5.5 kΩ at 1 GHz and 2 GHz, respectively.

When $R_D \ll |\omega(L_D + L_V) - 1/\omega C_D|$, $R \gg \omega L_M$ and $R \gg \omega L_R$, the circuit can be simplified as in Fig. 8(b), where the diode inductance becomes $L_D' = L_D + L_V + L_M$, and the lumped resistance is approximately replaced by

$$R' \sim R\left\{\frac{1-\omega^2(L_D+L_V+L_M)C_D}{1-\omega^2(L_D+L_V)C_D}\right\}^2. \tag{4}$$

Then the admittance Y_s of the circuit is written as,

$$Y_s = \frac{1}{R_D + j\left(\omega L_D' - \frac{1}{\omega C_D}\right)} + \frac{1}{R'} + \frac{1}{R_{\rm loss}} + j\omega C + \frac{1}{j\omega L}. \tag{5}$$

At the parallel resonance, $\mathrm{Im}(Y_s) = 0$ and we have

$$\frac{\omega^4}{\omega_1^2\omega_2^2} - \left(\frac{1}{\omega_0^2} + \frac{1}{\omega_1^2} + \frac{1}{\omega_2^2}\right)\omega^2 + 1 = 0, \tag{6}$$

where $\omega_0 \equiv 1/\sqrt{LC_D}$, $\omega_1 \equiv 1/\sqrt{L_D'C_D}$, and $\omega_2 \equiv 1/\sqrt{LC}$.

In deriving Eq. (6) we have used the condition $\omega^2 C_D^2 R_D^2 \ll 1$. Solving Eq. (6) for ω specifies two resonance frequencies, ω_{r1} and ω_{r2} ($\omega_{r1} < \omega_{r2}$), which are approximated when $\left(\omega_1^2+\omega_2^2+\omega_3^2\right)^2 \gg 4\omega_1^2\omega_2^2$, or roughly $C_D \gg C$ for the present case, as

$$\omega_{r1} \sim \left(\frac{1}{\omega_0^2}+\frac{1}{\omega_1^2}+\frac{1}{\omega_2^2}\right)^{-\frac{1}{2}} = \sqrt{\frac{1}{L(C+C_D)+L'_D C_D}}, \quad (7)$$

$$\omega_{r2} \sim \left(\omega_1^2+\omega_2^2+\omega_3^2\right)^{\frac{1}{2}} = \sqrt{\left(\frac{1}{L}+\frac{1}{L'_D}\right)\frac{1}{C}+\frac{1}{L'_D C_D}}, \quad (8)$$

where $\omega_3 \equiv 1/\sqrt{L'_D C}$. Note that the first resonance frequency has been modified from Eq. (3) by the existence of L'_D, and the second resonance frequency has appeared. By controlling the value of C_D from 12 pF to 0.67 pF on the present EBG absorber, the first resonance frequency ω_{r1} can be varied from 700 MHz to 2.7 GHz, while the second resonance ω_{r2} from 6.23 to 6.85 GHz. (Note that for small C_D comparable to $C = 0.628$ pF, we need to use the exact solution to Eq. (6), instead of the approximate solution Eq. (7).) In the present study we focus on the first resonance, since the variable range of the second resonance frequency is unpractically small.

At the first resonance the surface impedance becomes purely resistive, R_s, as shown in Fig. 8(c),

$$R_s = \left.\frac{1}{Y_s}\right|_{\omega=\omega_{r1}} = \frac{1}{1/R_r + 1/R' + 1/R_{\rm loss}}, \quad (9)$$

where R_r is calculated at the first resonance, as

$$R_r = \frac{L}{C_D R_D}\left(\frac{1-\omega_{r1}^2/\omega_1^2}{1-\omega_{r1}^2/\omega_2^2}\right) \sim \frac{L}{C_D R_D}\frac{1+C/C_D}{1+L'_D/L}. \quad (10)$$

When $C_D \gg C$, $\omega_{r1}^2 \sim 1/\left(L+L'_D\right)C_D$ from Eq. (7), so that Eq. (10) is further reduced to $R_r \sim \omega_{r1}^2 L^2/R_D$; the resistance becomes smaller at lower resonance frequencies. In the present case, for example, when $C_D = 0.67$ pF and $\omega_{r1} = 2.7$ GHz, $R_D = 1.0\,\Omega$ gives $R_r \sim 2.2\,\mathrm{k}\Omega$. When $C_D = 12$ pF and $\omega_{r1} = 700$ MHz, $R_D = 2.2\,\Omega$ yields $R_r \sim 32\,\Omega$. Thus, even a small series resistance R_D of the varactor is translated into a much larger resistance R_r [16]. For the matching condition to be satisfied (i.e., the good absorption to be achieved) over the resonance frequency range of interest, $R_r > 377\,\Omega$ should be maintained, since both the dielectric loss $R_{\rm loss}$ and the lumped resistors R inserted in parallel with R_r reduce the resultant surface resistance, $R_s < R_r$. Unfortunately for the present EBG absorber $R_r > 377\,\Omega$ was achieved just above 1.9 GHz. In the present study the value of lumped resistors R was chosen as $620\,\Omega$, which gives $R_s \sim 377\,\Omega$ at the resonance frequency around 2.62 GHz (when $C_D = 0.72$ pF), from Eqs. (9) and (10).

3.3 Simulation Model

The absorption characteristics of the EBG absorber described in Sect. 3.1 was also analyzed by the electromagnetic simulation by using CST Microwave Studio commercial software. A linearly polarized plane wave was incident normally on the EBG surface. A square area containing four unit cells of the absorber was modeled by defining the periodic boundary condition, which corresponds to simulating infinitely extending periodic unit cells.

3.4 Measurement and Performance Evaluation

We measured the actual absorption performance of the fabricated EBG absorber in an anechoic chamber, and compared it with those obtained in the equivalent circuit analysis and the simulation. Reflection loss measurements were carried out using a vector network analyzer (Anritsu, 37297C) and a double ridged waveguide horn antenna (ETS, 3115: 1–18 GHz) which was placed 1.5 meters above the absorber. A dielectric lens was inserted between the horn antenna and the EBG absorber to ensure the measurement of reflection from the EBG absorber with the size of 347 mm square which was not much larger than the wavelength. Figure 9 plots the measured profiles of reflection magnitude by solid lines, while the profiles obtained in the equivalent circuit analysis and the simulation are plotted by broken and gray lines, respectively. In either case four representative profiles are plotted for the varactor capacitances fixed as $C_D = 3.35$ pF, 1.72 pF, 1.09 pF and 0.72 pF, which correspond to the resonance frequencies of 1.3 GHz, 1.8 GHz, 2.2 GHz and 2.62 GHz, respectively. In the parentheses by the capacitance values are indicated the varactor resistances R_D at the corresponding resonance frequencies.

For each of the capacitance values, the reflection profile calculated by the equivalent circuit analysis agrees well to that obtained in the simulation, which validates the equivalent circuit in Fig. 8. On each curve, the absorption becomes maximum (the reflection becomes minimum) at the resonance frequency determined by the value of C_D. As was described in Sect. 3.2, the amount of absorption becomes largest ($S_{11} \sim -30$ dB) at the resonance frequency of 2.62 GHz for the case of $C_D = 0.72$ pF, where the surface resistance R_s of the EBG absorber becomes almost $377\,\Omega$ which matches the incident wave impedance. The maximum absorption becomes smaller when the resonance frequency becomes lower, since the surface resistance R_s be-

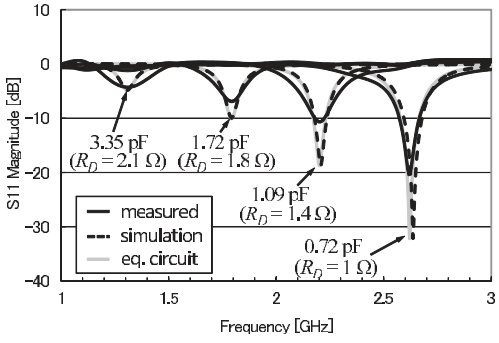

Fig. 9 Reflection magnitudes of the fabricated EBG absorber.

comes smaller than 377 Ω so that the impedance mismatch becomes larger (see Sect. 3.2); R_s = 291 Ω, 197 Ω and 97 Ω at $\omega_{r1}/2\pi$ = 2.2 GHz, 1.8 GHz and 1.3 GHz, respectively.

The measured profiles (solid lines), on the other hand, exhibit the maximum absorption at the resonance frequencies consistent with the theoretical profiles obtained by the equivalent circuit analysis and the simulation (broken and gray lines). However, the amount of absorption was observed to be less than the theoretical one at each resonance frequency. This is likely caused by that, in the measurement of the reflection profiles, the time gate used by the vector network analyzer to extract the reflected waves was too short (3.3 nsec) to obtain the prominent absorption peaks at the resonance frequencies.

As mentioned in Sect. 3.2, to achieve the sufficient absorption over a certain range of resonance frequencies, the equivalent resistance R_r of the varactor must be at least greater than 377 Ω. From Eq. (10), one way to make it so is to adopt the varactor with the resistance R_D as small as possible. The second way is to reduce the varactor capacitance C_D, but it is difficult to make it smaller than a fraction of pF because of the existence of the stray capacitance of a varactor chip package. Last but not least, it is possible to increase the inductance of the EBG structure L, which is theoretically proportional to the thickness of the substrate. Since the resonance frequency is determined by C_D and L, appropriate values should be carefully chosen in the design of the tunable EBG absorber.

4. Measurement Results of RF Power Distributions

4.1 RF Power Imager with an EBG Absorber

Figure 10 shows a block diagram of the RF power imager developed in the present study. As explained in Sect. 2.2, the RF power distribution incident on the surface was detected by an array of power detectors placed on the backside of the EBG absorber. A total of 128 power detectors were almost uniformly distributed over the absorber; half of them (64 detectors) were arranged in a 8×8 matrix to measure the x-polarization, while the other half (64 detectors) were also in a 8×8 matrix for the y-polarization. A logarithmic detector (Analog Devices, ADL5513) was used as the power detector, which had the measurable input power range from −70 dBm to +10 dBm. The frequency bandwidth of ADL5513 was from 1 MHz to 4 GHz, which covered the first resonance frequency range of the fabricated EBG absorber (700 MHz–2.7 GHz). The differential input of each ADL5513 on the backside was connected to the face-to-face sides of two adjacent patches on the surface with vias as in Fig. 5. In fact, the impedance of each power detector as seen from the sides of the surface patches was adjusted to be almost 620 Ω, so that the lumped resistor (620 Ω) was completely replaced by the power detector at each of the power detection points.

The detected RF power distribution was then A/D-converted and transferred to a PC, and displayed as a 2-d color-map image on its screen. The PC also specified the bias voltage to be supplied to the varactor diodes on the EBG absorber, thereby controlling the resonance (absorption) frequency. The rate of updating the power distribution images was set as about 30 images/second.

4.2 Tuning of Resonance Frequencies

By using the RF power imager described in Sect. 4.1, RF power distributions radiated from an antenna were measured and evaluated. The experimental setup is shown in Fig. 11. Radio waves (0 dBm) were transmitted from a standard half-wavelength dipole antenna (Anritsu, MP651B: 470 MHz–1.7 GHz) with a horizontal polarization (in the x-direction) in an anechoic chamber. The radio waves were then absorbed by the EBG absorber put on a vertical plane (the x-y plane) at a distance d from the transmitter (TX). The absorbed power distributions were measured by the power detectors for horizontal polarization (P_x), since in this configuration the absorption mainly occurs by the horizontal resistors R_x (see Fig. 4). The center of the EBG surface is taken as the coordinate origin.

While the transmitted frequency was fixed, the bias voltage applied to the varactors was swept so that the resonance frequency of the EBG absorber was varied. Figure 12 shows the amount of power absorbed and measured almost at the center of the EBG absorber, which corresponded to the case of almost normal incidence. The horizontal axis shows the bias voltage which was almost proportional to

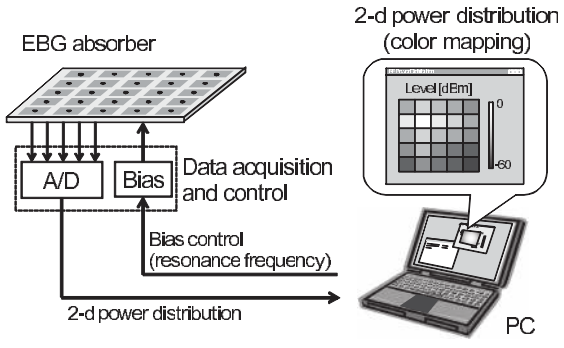

Fig. 10 RF power imager.

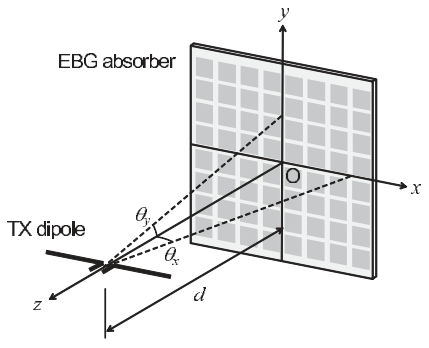

Fig. 11 Measurement of RF power radiated from a dipole antenna.

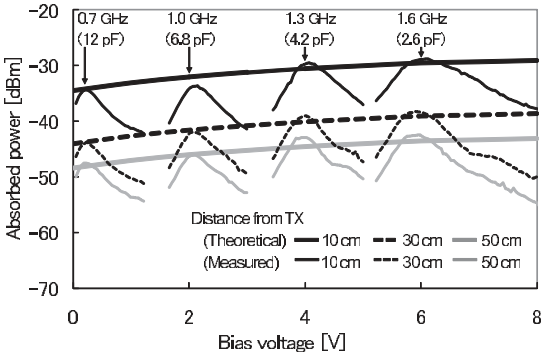

Fig. 12 RF power measured by the RF power imager.

the resonance frequency; as indicated in the figure, the bias voltages of 0.2, 2, 4 and 6 V corresponded to the resonance frequencies of 0.7, 1.0, 1.3 and 1.6 GHz (the varactor capacitance values were 12, 6.8, 4.2 and 2.6 pF), respectively. Three continuous thick curves spanning over the entire bias voltage range show the theoretically expected amounts of the absorbed power (i.e., the power incident and absorbed on the area of a^2; see Eq. (2)), $P = P_d|A|^2$, where $P_d = P_t G_a a^2/4\pi d^2$, $P_t = 1$ mW (0 dBm) is the transmitted power, and $G_a = 1.64$ is the gain of the dipole. In calculating the power absorption coefficient $|A|^2 = 1 - |(Z_s - \eta_0)/(Z_s + \eta_0)|^2$, the surface impedance Z_s was evaluated by the equivalent circuit analysis in Sect. 3.2, for the case of the transmitted frequency equal to the resonance frequency. Solid, broken and gray lines are for the cases that the distances between the transmitter and the EBG absorber are $d = 10$, 30 and 50 cm, respectively. The absorption decreases with increasing distance, according to the radiated power density decreasing with d^{-2} (here we used the far-field approximation). At each distance, the amount of absorption becomes smaller as the voltage (so the resonance frequency) becomes lower, because of the increase in mismatch between the EBG surface impedance and the incident wave impedance (see Sect. 3.2). On the other hand, twelve isolated thin curves in Fig. 12 represent the measured (absorbed) power profiles at the three distances when the four fixed frequencies, 0.7, 1.0, 1.3 and 1.6 GHz, were transmitted independently of each other. Each of these curves takes a maximum at the resonance frequency specified by the bias voltage being equal to the transmitted frequency. Thus the frequency of unknown radio sources are estimated by sweeping the bias voltage. The amount of measured power at each maximum is consistent with the corresponding theoretical value, which validates the power detection principle proposed in the present study. The small errors of 1–2 dB are considered to be caused by the standing waves between the transmitter and the EBG absorber, which were possibly created due to imperfect absorption on the EBG absorber.

4.3 Measurement of Spatial Distributions

Figure 13 presents the RF power distributions measured by the power detectors for horizontal polarization (P_x) on the

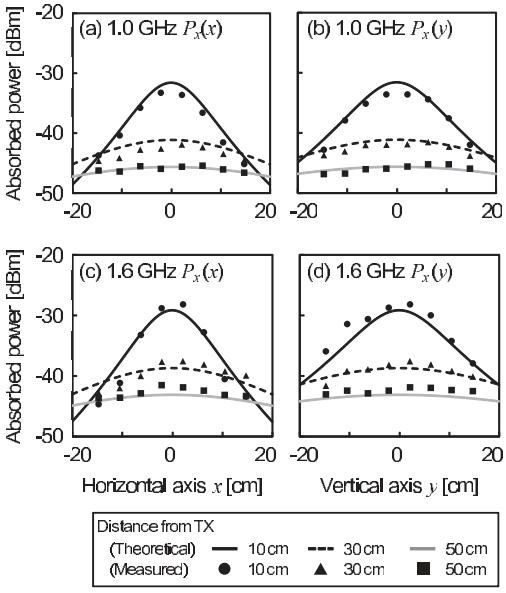

Fig. 13 RF power distributions measured by the RF power imager.

EBG absorber, which was tuned to the transmitted frequencies. Figures (a) and (b) show the 1.0 GHz power profiles of horizontal polarization along the x- and y-axes, $P_x(x)$ and $P_x(y)$, while (c) and (d) are the 1.6 GHz profiles. In each figure the theoretical profiles at the distances of 10, 30 and 50 cm from the transmitter are represented by solid, broken and gray lines, respectively. Here the theoretical profiles were calculated as follows. A far-field spherical wave radiated by the dipole antenna is approximated as obliquely incident plane waves on the EBG surface. More rigorous treatment requires an evaluation of the spherical wave incidence to the EBG surface, which is beyond the scope of the present paper. In the configuration shown in Fig. 11, the TM- and TE-mode power profiles which is incident on the x- and y-axes on the EBG surface and measured by the power detectors are expressed respectively as,

$$P_{\mathrm{TM}}(x) = P_d \cos^3\theta_x \, D_x^2(\theta_x) \, |A_{\mathrm{TM}}|^2, \tag{11}$$

$$P_{\mathrm{TE}}(y) = P_d \cos^3\theta_y \, D_y^2(\theta_y) \, |A_{\mathrm{TE}}|^2, \tag{12}$$

where $D_x(\theta_x) = \cos\{(\pi/2)\sin\theta_x\}/\cos\theta_x$ and $D_y(\theta_y) = 1$ represent the directivities of the dipole, and θ_x and θ_y are the angles of incidence onto the x- and y-axes, respectively (see Fig. 11). The power absorption coefficients for the TM- and TE-modes are calculated as

$$|A_{\mathrm{TM}}|^2 = 1 - |\Gamma_{\mathrm{TM}}(\theta_x)|^2 = 1 - \left|\frac{Z_s - \eta_0\cos\theta_x}{Z_s + \eta_0\cos\theta_x}\right|^2, \tag{13}$$

$$|A_{\mathrm{TE}}|^2 = 1 - |\Gamma_{\mathrm{TE}}(\theta_y)|^2 = 1 - \left|\frac{Z_s\cos\theta_y - \eta_0}{Z_s\cos\theta_y + \eta_0}\right|^2, \tag{14}$$

where Γ_{TM} and Γ_{TE} are the reflection coefficients for the TM- and TE-mode plane waves, respectively.

In Fig. 13 the measured values are plotted by black circles, triangles and squares for the distances of 10, 30 and 50 cm, respectively. The measured values are consistent

with those predicted by theory, even at the closest distance (d =10 cm) where the far-field approximation may not be sufficiently valid; $d > \lambda/2\pi$(=4.8 cm at 1 GHz) holds, but not $d >> \lambda/2\pi$. Small variations (up to a few dB) observed on each profile are again possibly caused by the standing waves due to imperfect absorption on the EBG absorber.

Thus the RF power distributions incident on the EBG absorber can be measured by the RF power imager. As the sensor scanning is not necessary, snapshots of the RF distributions can be obtained, even for impulsive RF signals and/or noises. The minimum detectable RF power is as low as −70 dBm. Since the power distribution absorbed on the EBG surface is detected, this imager is expected to cause little disturbance to the ambient electromagnetic environment during measurement, when good absorption is achieved at the distances where the far-field approximation is valid. Nevertheless it would be difficult to completely absorb the obliquely incident TM and TE waves, as their wave impedance depends on angles of incidence. Furthermore the oblique incidence may change the resonance (absorption) frequency of the EBG structure [6]. Use of a high-permittivity substrate will mitigate to some extent such an effect [22]. Another feature of the RF power imager is that, though no results were presented here, the incident polarizations (vertical and horizontal) are easily distinguished by evaluating the amounts of power measured by the vertical and horizontal power detectors.

From the viewpoint of RF power "imaging," the spatial resolution of power distribution measurement is also important. As described in Sect. 4.1, the RF power imager developed in the present study had 64 (=8×8) power detectors for each polarization. They were uniformly distributed in a matrix over the 347-mm square EBG absorber having 33×33 cells; the power detectors were placed at every four mushroom cells in each of x- and y-directions, so that the spatial resolution of the imager was 42 mm (four times the cell size of 10.5 mm). Since we detect the amounts of power absorbed by the individual resistors interconnecting the mushroom cells, the highest resolution of 10.5 mm (equal to the cell size) will be achieved by using the present EBG absorber, if the power detectors are installed at every mushroom cell. This resolution is much smaller than the wavelengths covered (43 cm and 11 cm at 700 MHz and 2.7 GHz, respectively), so that even spatial fading patterns created by the interference between two or more incident waves could be clearly visualized. Further higher-resolution imaging may be possible if the cell size is made smaller in the future study. It should be noted, however, that the power detection sensitivity will be degraded because less power will be absorbed by the smaller cell (see Eq. (2)).

5. Conclusion

A technique to measure RF power distributions by using an EBG absorber was proposed and evaluated. An EBG absorber was designed and fabricated, where the lumped resistors interconnecting the mushroom cells absorb the RF waves incident on the EBG surface at the resonance frequency, which is made tunable with varactor diodes (700 MHz–2.7 GHz). The absorption performance was examined by equivalent circuit analysis, simulations and measurements. It was shown that the existence of even a small varactor resistance significantly degraded the absorption performance especially at low frequencies. A matrix of power detectors were attached on the EBG absorber, to measure directly the RF power distribution (as low as −70 dBm) absorbed by the lumped resistors. The measured absorbed RF power distributions were found to be consistent with those expected by theory. Thus the proposed technique to measure the RF power distributions was validated.

Using the developed "RF power imager," the snapshots of even impulsive RF signal and/or noise power distributions can be captured and visualized in situ and in real-time, while the electromagnetic environment is virtually undisturbed by the EBG absorber. The polarization discrimination is also possible. Such a system is expected to be quite useful for measuring RF power distributions in various scenarios in the fields of EMC, antennas and propagation.

Acknowledgments

The authors would like to thank Dr. M. Ozaki for his valuable suggestions and discussions. We also thank Mr. T. Shimizu (now at NTT DoCoMo, Inc.), Mr. Y. Yamanaka (now at Mitsubishi Electric Corporation), Mr. S. Morita (now at Musasino Co., Ltd.), Mr. E. Tanaka and Mr. R. Tanaka of Kanazawa University for their help with the design, fabrication and measurement of the RF power imager. This study was supported by KAKENHI (21560444).

References

[1] K. Sasagawa, A. Kanno, T. Kawanishi, and M. Tsuchiya, "Live electrooptic imaging system based on ultraparallel photonic heterodyne for microwave near-fields," IEEE Trans. Microw. Theory Tech., vol.55, no.12, pp.2782–2791, Dec. 2007.
[2] J. Norgard and R. Musselman, "CEM code validation using infrared thermograms," 2004 International Symposium on Electromagnetic Compatibility, pp.637–640, June 2004.
[3] N. Chiyo, Y. Tanaka, T. Maeno, and A. Nishikata, "3-d electromagnetic field intensity measurement of microwave using an infrared 2-d lock-in amplifier," IEICE Trans. Commun. (Japanese Edition) B, vol.J91-B, no.12, pp.1744–1745, Dec. 2008.
[4] N. Engheta, "Thin absorbing screens using metamaterial surfaces," 2002 IEEE Antennas and Propagation Society International Symposium, vol.2, pp.392–395, June 2002.
[5] D.J. Kern and D.H. Werner, "A genetic algorithm approach to the design of ultra-thin electromagnetic bandgap absorbers," Microw. Opt. Technol. Lett., vol.38, no.1, pp.61–64, July 2003.
[6] S.A. Tretyakov and S.I. Maslovski, "Thin absorbing structure for all incidence angles based on the use of a high-impedance surface," Microw. Opt. Technol. Lett., vol.38, no.3, pp.175–178, Aug. 2003.
[7] A. Tennant and B. Chambers, "A single-layer tunable microwave absorber using an active FSS," IEEE Microw. Wirel. Compon. Lett., vol.14, no.1, pp.46–47, Jan. 2004.
[8] S. Simms and V. Fusco, "Thin radar absorber using artificial magnetic ground plane," Electron. Lett., vol.41, no.24, pp.1311–1313, Nov. 2005.

[9] H. Mosallaei and K. Sarabandi, "A one-layer ultra-thin meta-surface absorber," Proc. IEEE International Symposium on Antennas and Propagation, pp.615–618, July 2005.
[10] Q. Gao, Y. Yin, D.-B. Yan, and N.-C. Yuan, "A novel radar-absorbing-material based on EBG structure," Microw. Opt. Technol. Lett., vol.47, no.3, pp.228–230, Nov. 2005.
[11] T. Liang, L. Li, J.A. Bossard, D.H. Werner, and T.S. Mayer, "Reconfigurable ultra-thin EBG absorbers using conducting polymers," IEEE Antennas Propagation Soc. Int. Symp., 2005, vol.2B, pp.204–207, July 2005.
[12] J.H. Yap and C. Mias, "Tunable absorber based on electromagnetic band gap surface and a lossy resistance sheet," IEE Wideband and Multi-band Antennas and Arrays, 2005, vol.7, pp.171–175, Sep. 2005.
[13] S. Simms and V. Fusco, "Tunable thin radar absorber using artificial magnetic ground plane with variable backplane," Electron. Lett., vol.42, no.21, pp.1197–1199, Oct. 2006.
[14] D.J. Kern, J.A. Bossard, and D.H. Werner, "Design of reconfigurable electromagnetic bandgap surfaces as artificial magnetic conducting ground planes and absorbers," Proc. IEEE Antennas Propagation Soc. Int. Symp., 2006, pp.197–200, July 2006.
[15] D.J. Kern and D.H. Werner, "Magnetic loading of EBG AMC ground planes and ultrathin absorbers for improved bandwidth performance and reduced size," Microw. Opt. Technol. Lett., vol.48, no.12, pp.2468–2471, Dec. 2006.
[16] C. Mias and J.H. Yap, "A varactor-tunable high impedance surface with a resistive-lumped-element biasing grid," IEEE Trans. Antennas Propag., vol.55, no.7, pp.1955–1962, July 2007.
[17] F. Costa, A. Monorchio, and G. Manara, "Ultra-thin absorbers by using high impedance surfaces with resistive frequency selective surfaces," Proc. IEEE International Symposium on Antennas and Propagation, pp.798–801, June 2007.
[18] H.-T. Liu, H.-F. Cheng, Z.-Y. Chu, and D.-Y. Zhang, "Absorbing properties of frequency selective surface absorbers with cross-shaped resistive patches," Materials and Design, vol.28, no.7, pp.2166–2171, 2007.
[19] D.-U. Sim, J.-H. Kwon, S.-I. Kwak, and J.-H. Yun, "Design and analysis of novel broadband EM wave absorbers based on lossy EBG surface," IEEE 68th Vehicular Technology Conference, 2008, pp.1183–1186, Sept. 2008.
[20] N. Sonoda, T. Uno, and T. Arima, "Application of EBG structure to the reduction of undesired EM radiation," Proc. iWAT2008, pp.322–325, March 2008.
[21] A. Munir and V. Fusco, "Effect of surface resistor loading on high-impedance surface radar absorber return loss and bandwidth," Microw. Opt. Technol. Lett., vol.51, no.7, pp.1773–1775, July 2009.
[22] O. Luukkonen, F. Costa, C.R. Simovski, A. Monorchio, and S.A. Tretyakov, "A thin electromagnetic absorber for wide incidence angles and both polarizations," IEEE Trans. Antennas Propag., vol.57, no.10, pp.3119–3125, Oct. 2009.
[23] R. Miyazaki, A. Nishikata, T. Aoyagi, and Y. Kotsuka, "Tunable EM-wave absorber below 1 GHz using diode grid and its evaluation by large stripline," Proc. 2009 International Symposium on Electromagnetic Compatibility, no.24P1-2, pp.729–732, July 2009.
[24] T. Aoyagi, K. Murano, A. Nishikata, and Y. Kotsuka, "Metamaterial wave absorber to improve oblique incident characteristics," Proc. 2009 International Symposium on Electromagnetic Compatibility, no.24P1-3, pp.733–736, July 2009.
[25] F. Costa, A. Monorchio, and G. Manara, "Analysis and design of ultra thin electromagnetic absorbers comprising resistively loaded high impedance surfaces," IEEE Trans. Antennas Propag., vol.58, no.5, pp.1551–1558, May 2010.
[26] Y. Kotsuka, K. Murano, M. Amano, and S. Sugiyama, "Novel right-handed metamaterial based on the concept of "Autonomous Control System of Living Cells" and its absorber applications," IEEE Trans. Electromag. Compat., vol.52, no.3, pp.556–565, Aug. 2010.
[27] D. Sievenpiper, L. Zhang, R.F.J. Broas, N.G. Alexopolous, and E. Yablonovitch, "High-impedance electromagnetic surfaces with a forbidden frequency band," IEEE Trans. Microw. Theory Tech., vol.47, no.11, pp.2059–2074, Nov. 1999.
[28] D.F. Sievenpiper, J.H. Schaffner, H.J. Song, R.Y. Loo, and G. Tangonan, "Two-dimensional beam steering using an electrically tunable impedance surface," IEEE Trans. Antennas Propag., vol.51, no.10, pp.2713–2722, Oct. 2003.
[29] D. Sievenpiper, "Review of theory, fabrication, and applications of high-impedance ground planes," in Metamaterials, ed. N. Engheta and R.W. Ziolkowski, pp.287–311, Wiley-IEEE Press, 2006.
[30] Infineon Technologies AG, "Silicon Tuning Diodes BB833 (datasheet)," April 2007. Available at http://www.infineon.com

Satoshi Yagitani received his B.E., M.E., and Ph.D. degrees in electrical and computer engineering from Kanazawa University, Japan, in 1988, 1990 and 1993, respectively. Since 1993, he has been with Graduate School of Natural Science and Technology, Kanazawa University, where he is now a Professor of radio wave science and engineering. From 1997 to 1998, he was a visiting researcher at the University of Minnesota, USA. His research interests are measurement and visualization of electromagnetic fields, development of electromagnetic sensors, and analysis of plasma wave propagation in geospace with scientific spacecraft observations. He is a member of the IEEE, the Society of Geomagnetism and Earth, Planetary and Space Sciences (SGEPSS), and the American Goephysical Union (AGU). He was awarded the Ishikawa Prize for the promotion of industrial and academic collaboration in 2001.

Keigo Katsuda received his B.E. and M.E. degrees in information and systems engineering from Kanazawa University in 2009 and 2011, respectively. He was engaged in the research of the RF imager with an EBG absorber. He is now with Shibuya Kogyo Co., Ltd.

Masayuki Nojima received his B.E. degree in information and systems engineering from Kanazawa University in 2010. He is now studying for his M.E. degree at Kanazawa University. He has been engaged in the research of EBG absorbers.

Yoshiyuki Yoshimura received his B.E. and M.E. degrees in Mechanical Systems Engineering from Nagaoka University of Technology, Japan, in 1988 and 1990, respectively, and his Ph.D. degree in Mathematics and Information Science from Kanazawa University, Japan, in 2003. Since 1990, he has been with Industrial Research Institute of Ishikawa, Electronics and Information Department, where he is now a Chief Researcher. He is engaged in the research of electromagnetic interference/compatibility (EMI/EMC) problems.

Hirokazu Sugiura received his B.E. and M.E. degrees in electrical and computer engineering from Kanazawa University, Japan, in 2000 and 2002. Since 2007, he has been with Industrial Research Institute of Ishikawa, Electronics and Information Department, where he is now a Chief Engineer. He is engaged in the research of electromagnetic interference/compatibility (EMI/EMC) problems.